Reversible Transition between the Surface Trimer and Membrane-Inserted Monomer of Annexin 12[†]

Alexey S. Ladokhin*[,‡] and Harry T. Haigler[§]

Department of Biochemistry and Molecular Biology, Kansas University Medical Center, Kansas City, Kansas 66160-7421, Department of Physiology and Biophysics, University of California, Irvine, California 92697-4560

Received October 13, 2004; Revised Manuscript Received December 14, 2004

ABSTRACT: Under mildly acidic conditions, annexin 12 (ANX) inserts into lipid membranes to form a transbilayer pore [Langen, R., et al. (1998) *Proc. Natl. Acad. Sci. U.S.A. 95*, 14060]. In this study, we have addressed the question of the oligomeric state of ANX in this transbilayer conformation by means of Förster-type resonance energy transfer (FRET). Two single-cysteine mutants (K132C and N244C) were labeled with either Alexa-532 (donor) or Alexa-647 (acceptor). The labels were positioned at the sites thought to be on the cis side of the known transmembrane regions [Ladokhin, A. S., et al. (2002) *Biochemistry 41*, 13617]. If the pore were comprised of an annexin oligomer, efficient energy transfer should be observed. Fluorescence excitation spectra of several mixtures of donor- and acceptor-labeled ANX were recorded under various conditions. Spectroscopic hallmarks of oligomerization-related FRET were established by following a well-documented transition of ANX from the soluble monomer to surface trimer upon addition of calcium at neutral pH. These hallmarks, however, were not detected for the membrane-inserted form of ANX at pH 4.5, suggesting that the transbilayer form is a monomer. This implies that the pore is formed by several transmembrane regions of the same ANX molecule. FRET and other fluorescence experiments demonstrate that the transitions between the surface trimer and membrane-inserted monomer are reversible. This reversibility, in combination with the absence of oligomerization in the water-soluble and inserted state, makes ANX a good experimental model for thermodynamic studies of folding and stability of membrane proteins.

Protein translocation and insertion across cellular membranes are important functions, generally managed by complex multiprotein assemblies (*1*−*3*). In some instances, however, they can be achieved spontaneously, in response to changes in environment (e.g., acidification), as in the case of such bacterial toxins as botulinum and diphtheria toxin (*4*−*8*). The structural and thermodynamic details of either translocon-assisted or spontaneous membrane insertion of proteins are far from being understood. One of the reasons the studies of folding and stability of membrane proteins lag far behind those of their soluble counterparts is the lack of appropriate experimental models. Although it is likely that most proteins in the cell require molecular chaperones for efficient folding, the main thermodynamic principles that govern folding of soluble proteins were established from thorough studies of spontaneously folding proteins [e.g., barnase (*9*), apomyoglobin (*10*), and staphylococcal nuclease (*11*, *12*)]. Our recent study of the spontaneous membrane insertion and folding of the diphtheria toxin T-domain suggested that a similar strategy can be applied to thermodynamic studies of membrane proteins (*13*). The demonstrated reversibility of insertion of the T-domain had opened doors to the systematic exploration of the thermodynamics of the process, yet the T-domain might not be the optimal vehicle for such studies, as it tends to aggregate in solution at acidic pH. Recently, it has been demonstrated that annexin 12 (ANX)[1] undergoes spontaneous transmembrane insertion at low pH (*14*), thus making it a potentially attractive experimental model for the study of structural and thermodynamic aspects of membrane protein insertion and folding.

Annexins are a structurally conserved family of proteins implicated in a variety of membrane-related functions, including vesicular trafficking, membrane fusion, and ion channel formation (*15*, *16*). They are also associated with several diseases known as "annexinopathies" (*17*, *18*). The hallmark of annexin function is reversible Ca^{2+}-dependent binding to membranes (*15*, *16*). High-resolution crystal structures of the soluble forms of several different annexins reveal a common fold consisting of four repeats (*19*). All repeats have essentially the same backbone fold and consist

[†] This research was supported by NIH Grants GM-069783 (A.S.L.) and GM-55651 (H.T.H.).

* To whom correspondence should be addressed. Phone: (913) 588-0489. Fax: (913) 588-7440.

[‡] Kansas University Medical Center.

[§] University of California.

[1] Abbreviations: ANX, annexin 12; ANX-132, ANX-144, and ANX-244, single-cysteine mutants K132C, S144C, and N244C of annexin 12, respectively; ANX-144NBD, NBD-labeled mutant K132C; ANX-132D and ANX-244D, single-cysteine mutants labeled with the FRET donor dye (Alexa-532); ANX-132A and ANX-244A corresponding single-cysteine mutants labeled with the FRET acceptor dye (Alexa-647); FRET, Förster resonance energy transfer; LUV, extruded large unilamellar vesicles 100 nm in diameter; NBD, 7-nitrobenz-2-oxa-1,3-diazol-4-yl; POPC, palmitoyloleoylphosphatidylcholine; POPG, palmitoyloleoylphosphatidylglycerol; PC, egg yolk phosphatidylcholine; PS, bovine brain phosphatidylserine; PS/PC, a 2:1 weight ratio mixture of PS and PC; POPG/POPC, 1:3 molar mixture of POPG and POPC.

10.1021/bi047805u CCC: $30.25
Published on Web 02/08/2005

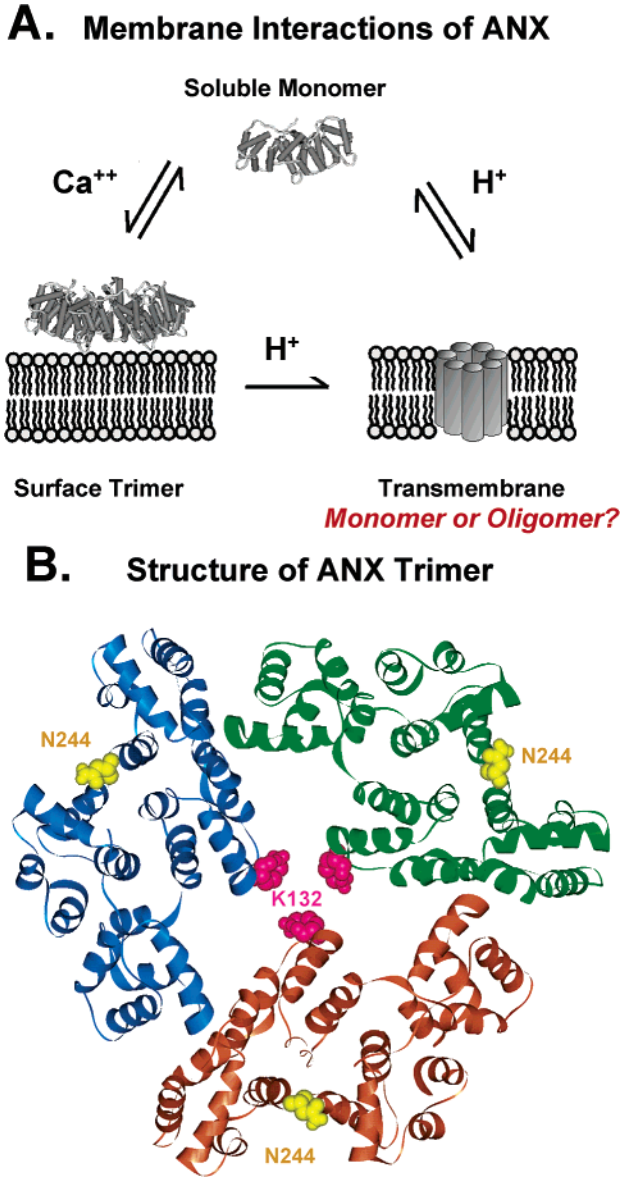

FIGURE 1: (A) Schematic representation of membrane interactions of annexin 12 (*29*). At neutral pH in the presence of Ca^{2+}, annexin undergoes a well-characterized transition from a water-soluble monomer to a membrane surface-bound trimer, without a change in tertiary structure (*24*). At acidic pH, annexin refolds and inserts to form a transmembrane pore (*14*). It is not known whether this pore is composed of the protein monomer or multimer. (B) Proposed structure of the ANX trimer in Ca^{2+}-bound membrane form (*24*) based on a crystallographic structure (*40*). Two single-cysteine mutants were used in this study, K132C and N244C. The distance between α-carbons in different subunits is 12 Å for K132 (magenta) and 64 Å for N244 (yellow).

of five α-helices (labeled A−E) joined by short connecting loops (*19*). The Ca^{2+} binding sites are located in or near the loops that connect the A and B helices and the D and E helices. Ca^{2+}-dependent membrane binding of annexins is mediated by a Ca^{2+} bridge between these loops and the headgroups of membrane phospholipids (*20*). Annexins are monomers in solution, but some annexins form trimers upon Ca^{2+}-dependent binding to membranes (*21*−*24*). ANX is one of the annexins that forms trimers (illustrated in Figure 1). Only subtle changes in the backbone fold of ANX occur when soluble monomers assemble into trimers on the surface of membranes (*25*, *26*).

Although the classical function of annexins is reversible Ca^{2+}-dependent binding to membranes, a growing body of literature describes a form of annexins that cannot be extracted from biological membranes by chelating Ca^{2+} (*27*). Ca^{2+}-independent membrane association of ANX was induced by mildly acid pH (*14*, *28*, *29*) and involved global refolding of the protein (*26*). Refolding occurred in the pH range of approximately 5−7 and was dependent on the phospholipid composition of the bilayer (*26*). A nitroxide scan of a region of ANX that includes the Ca^{2+}-binding loop between the D and E helix of the second repeat showed that the helix−loop−helix hairpin refolded at low pH and formed a continuous transmembrane helix consisting of residues 138−158 (*14*). This transmembrane helix, along with other unidentified amphipathic helices, formed an aqueous pore with ion channel activity (*14*, *28*). A fluorescence spectroscopy study detected an intermediate in the refolding process and established the topology of the 138−158 transmembrane helix (*30*). Another nitroxide scan recently has shown that the helix−loop−helix region in the third repeat of ANX (residues 219−239) also refolded and formed a transmembrane helix at low pH in the absence of Ca^{2+} (J. M. Isas, H. T. Haigler, and R. Langen, unpublished results). Taken together, these studies establish that ANX can form a transmembrane pore but did not address the question of whether the pore was formed by several amphipathic helices from the same protein molecule or by an oligomer in which different molecules combined to form the pore.

Here we use the FRET experimental approach to address the issue of the oligomeric state of the transmembrane form of ANX at low pH. Using the single-cysteine K132C mutant of ANX, donor or acceptor dyes were placed near the transmembrane helix formed by residues 138−158. Mixtures of the donor and acceptor pair were inserted into phospholipid vesicles at low pH and monitored for fluorescence energy transfer indicative of oligomer formation. The N244C mutant also was labeled near the transmembrane helix formed by residues 219−239. Since previous studies established that positions 132 (*30*) and 244 (J. M. Isas, H. T. Haigler, and R. Langen, unpublished results) are on the cis side of the bilayer, dyes attached to these positions did not have to cross the bilayer during the insertion process which thus reduced the risk that fluorescent labeling would interfere with the process being studied.

Using these two donor−acceptor pairs of fluorescently labeled ANX, we first established the spectroscopic hallmarks of FRET using the well-known Ca^{2+}-dependent ANX trimer on membrane interfaces (Figure 1B). In the trimer, the distance between the α-carbons of position 132 is 12 Å and the distance between the α-carbons of position 244 is 64 Å. Second, we applied the same experimental protocol to a low-pH transmembrane state of ANX, finding it to be a monomer. This implies that in addition to the two known D−E transmembrane regions of ANX, other regions of the same molecule form the remainder of the pore structure. And finally, to determine whether the interaction of ANX with bilayers is a suitable model system for thermodynamic analysis, we examined the reversibility of the refolding and oligomeric states depicted in Figure 1A.

EXPERIMENTAL PROCEDURES

Materials. POPC, POPG, PC (a mixture of phosphatidylcholine lipids from egg yolk, catalog no. 840051), and PS (a mixture of phosphatidylserine lipids from bovine brain, catalog no. 84032) were purchased from Avanti Polar Lipids (Alabaster, AL). INBD, Alexa-532 C_5 meleimide, and Alexa-647 C_2 maleimide were purchased from Molecular Probes (Eugene, OR). Two buffers, acidic and neutral, were used in this study. The acidic buffer (pH 4.5) was composed of 10 mM sodium acetate and 50 mM NaCl, and the neutral buffer (pH 7.0) was composed of 10 mM HEPES and 50 mM NaCl. Both contained 1 mM EGTA.

Labeling of Single-Cysteine Mutants of ANX. Single-cysteine mutations were introduced into Cys-less ANX at positions 132, 144, and 244, and the mutants were isolated as described previously (*14*). The ANX-144 mutant was labeled with NBD as described previously (*30*). Labeling with Alexa dyes was performed using a standard procedure for the thiol-reactive maleimide derivatives (*31*). Typically, 1 mg of maleimade derivative of the dye was dissolved into a 0.2 mL of a 50 μM solution of protein in 10 mM HEPES (pH 7.0) containing 50 mM KCl and 1 mM EDTA. The reaction mixture was incubated overnight at 4 °C. Excess dye was removed by gel filtration chromatography (PD-10 column) followed by a series (five to seven) of centrifugations using a Microcon YM-10 concentrator, until the solution coming through the concentrator did not contain any dye, as assayed by absorbance spectroscopy. The concentration of labeled annexin was estimated from peak absorbance measurements, with the assumption that the extinction coefficients are the same as for the free dyes: 75 000 M^{-1} cm^{-1} for Alexa-532 and 265 000 M^{-1} cm^{-1} for Alexa-647.

Sample Preparation. Large unilamellar vesicles with a diameter of 0.1 μm were prepared by extrusion (*32*, *33*) using the following lipid mixtures: a 2:1 (w:w) mixture of bovine brain phosphatidylserine and egg yolk phosphatidylcholine (PS/PC) and a 1:3 molar mixture of POPG and POPC (POPG/POPC). Membrane insertion was induced by adding the stock solutions of proteins and LUV to 1 mL of pH 4.5 buffer. For Ca^{2+}-dependent binding, membrane interactions were initiated at pH 7 by adding 0.3 mM Ca^{2+} in excess of EGTA. The samples typically contained 5 nM annexin labeled with the donor dye (Alexa-532) and 10 nM annexin labeled with the acceptor dye (Alexa-647) and 0.1 mM lipid vesicles. In the course of reversibility experiments, the pH of the sample was changed by adding appropriate aliquots of a 0.4 M solution of HEPES (to increase the pH to 7) or a 0.5 M solution of sodium acetate (to lower the pH to 4.5).

Fluorescence. Fluorescence was measured using an SLM 8100 steady-state fluorescence spectrometer [Jobin Yvon, Edison, NJ (formerly SLM/AMINCO, Urbana, IL)] equipped with double-grating excitation and single-grating emission monochromators. The measurements were taken in 4 mm $\times$ 10 mm cuvettes oriented with the long axis parallel to the excitation beam. The temperature was maintained at 25 °C using a circulating water bath. Cross-orientation of polarizers was used (excitation polarization set to vertical, emission polarization set to horizontal) to minimize the scattering contribution from vesicles and to eliminate spectral polarization effects in monochromator transmittance. Fluorescence excitation spectra of dye-labeled annexins were obtained by averaging 5−10 scans collected over a 470−660 nm range using 1 nm steps. The emission monochromator was set at 680 nm. Excitation slits were 8 nm, and emission slits were 16 nm. Emission spectra were collected over a 520−720 nm range using excitation at 470 nm, excitation and emission slits of 8 nm, a vertically oriented emission polarizer, and a horizontally oriented excitation polarizer. Because energy transfer causes depolarization of emission, the use of cross-oriented polarizers increases the sensitivity of spectral measurements to the presence of FRET.

Resonance Energy Transfer. The energy transfer efficiency E depends on the distance r between the donor (NBD) and acceptor (lysoUB) and the Förster distance R_0:

$$E = R_0^6/(R_0^6 + r^6) \quad (1)$$

The Förster distance is generally computed from (*34*)

$$R_0 = 9.79 \times 10^3(\kappa^2 n^{-4} \phi_d J)^{1/6} \text{ Å} \quad (2)$$

where κ^2 describes the relative orientations of the acceptor and donor, n is the refractive index of the medium, ϕ_d is the quantum yield of the donor, and J is the integral of the spectral overlap between the donor emission and the acceptor absorption. If the donor and acceptor are isotropically oriented, as frequently assumed, then $\kappa^2 = {}^2/_3$. The assumptions related to the application of the energy transfer method in membrane systems and to calculations of R_0 have been addressed in the literature (*35*−*38*). In the method outlined here, however, the precise value of R_0 is less important, because we use the well-known structure of the Ca^{2+}-induced trimer of ANX as a reference system. Given the variations in the quantum yield of donor in various environments, we have estimated R_0 for the Alexa-532−Alexa-647 donor−acceptor pair to be between 55 Å (for ANX-132 in transmembrane form) and 60 Å (for most other conditions).

RESULTS

Spectral Properties of Donor- and Acceptor-Labeled ANX. The fluorescence emission spectrum of Alexa-532 overlaps with the absorbance spectrum of Alexa-647 (Figure 2), making these fluorophores a convenient donor−acceptor FRET pair with a relatively large R_0 of ~55−60 Å (see Experimental Procedures). Emission spectra of the donor and acceptor are well-separated, as are their excitation spectra. This greatly minimizes the direct contribution of the donor to the acceptor's excitation spectrum and that of the acceptor to the donor's emission spectrum, which is a general problem of FRET experiments. In our case, however, it was possible to achieve virtually ideal photoselection of either the donor or acceptor by using appropriate excitation or emission wavelengths (marked with arrows in Figure 2). Only donor molecules (cyan trace) can be excited with the 470 nm light, while the absorbance of the acceptor (red trace) is negligible. Similarly, only acceptor molecules (magenta trace) contribute to emission at 680 nm, while the contribution of donor emission (blue trace) is vanishingly small. This spectral separation simplifies interpretation of the data and increases the sensitivity of spectral measurements to FRET.

Establishing Spectroscopic Hallmarks of Oligomerization Using Known Ca^{2+}-Dependent Trimer Formation of ANX. Figure 3 summarizes the spectroscopic responses of dye-

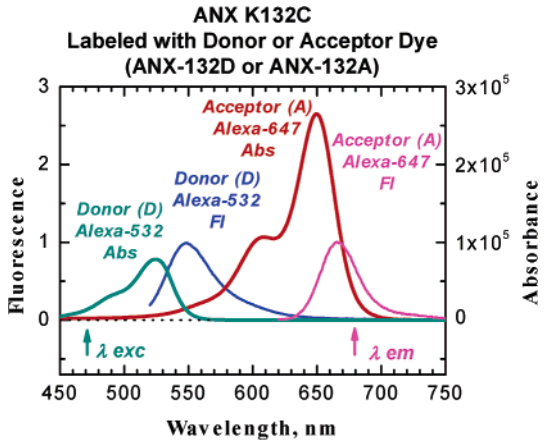

FIGURE 2: Spectroscopic properties of annexin-attached dyes used in this study. ANX-132 was labeled with either Alexa-532 or Alexa-647, and the spectra were recorded in buffer at pH 7.0. The overlapping emission spectrum of Alexa-532 (blue trace) and the absorbance spectrum of Alexa-647 (red trace) make these dyes a Förster resonance energy transfer (FRET) donor−acceptor pair with an R_0 of ~55−60 Å. At the same time, the spectral separation between the donor (cyan trace) and acceptor (red trace) absorbance allows for selective excitation of the donor dye using an excitation wavelength of 470 nm (marked with a cyan arrow). Similarly, the emission of the acceptor (magenta trace) can be selectively measured at 680 nm (marked with a magenta arrow).

labeled mutants of ANX to formation of a trimer (*24*) on membrane interfaces induced by addition of calcium (see the scheme in Figure 1A). Two single-cysteine mutants, K132C and N244C (Figure 1B), were labeled with either the donor dye (D), Alexa-532, or the acceptor dye (A), Alexa-647. Excitation (top panels in Figure 3) and emission spectra (bottom panels) were measured using the samples containing a 1:2 ratio of donor-labeled and acceptor-labeled ANX under various conditions. At neutral pH in the absence of Ca^{2+}, the excitation spectra of the ANX-D/ANX-A mixture coincide with that of the acceptor alone and emission spectra with that of the donor. This indicates the absence of FRET, as indeed is expected for a monomeric protein. Addition of Ca^{2+} in the presence of membranes results in the appearance of a donor-associated excitation peak and an acceptor-associated emission peak (marked with arrows in Figure 3). In addition, the emission intensity of the donor decreases due to the transfer of energy to the acceptor. These spectral changes result from efficient FRET associated with the formation of an ANX trimer. The changes can be totally reversed by chelating Ca^{2+} with EGTA (dashed curves).

In the case of ANX-244, the formation of the trimer did not affect the intensity of the donor. In the case of ANX-132, however, a substantial quenching was observed (Figure 3, top right panel, thick solid line). This quenching is not associated with the energy transfer from the donor to acceptor and is also observed for a sample containing only the acceptor and, to a lesser extent, for a sample containing only the donor (data not shown). It is likely that this quenching originates from the dyes attached to different subunits being very close to each other in the trimer (Figure 1B). To account

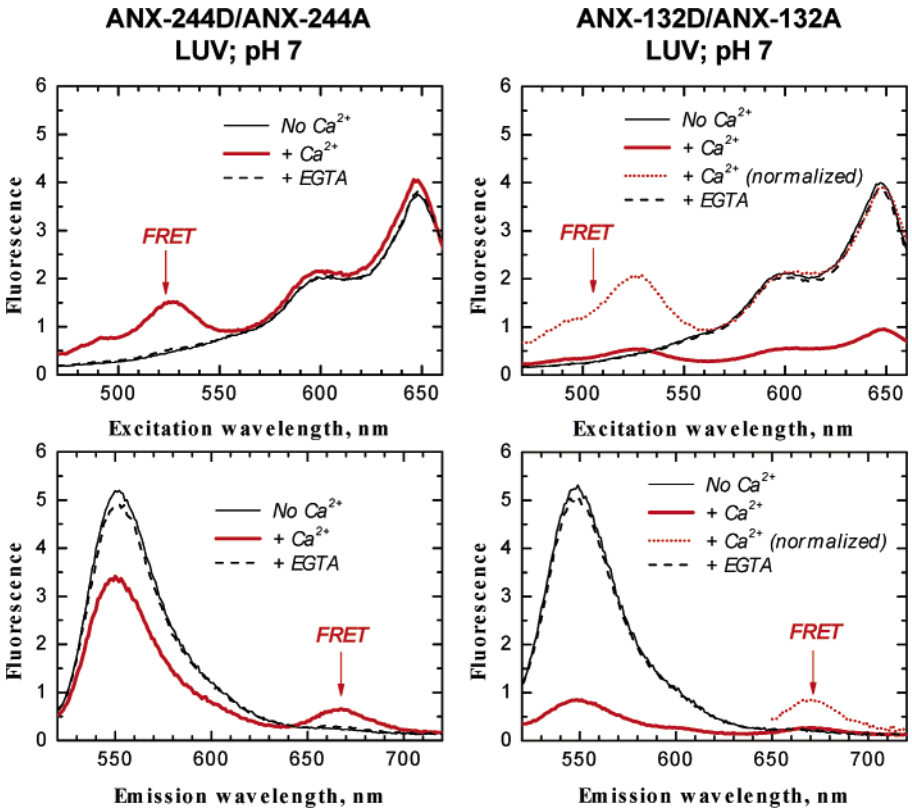

FIGURE 3: FRET experiment using the Ca^{2+}-bound annexin trimer (*24*) to establish the spectroscopic hallmarks of oligomerization. Excitation (top panels) and emission (bottom panels) spectra are measured for a mixture of donor- and acceptor-labeled annexin mutants N244C (left panels) and K132C (right panels). Addition of Ca^{2+} in the presence of POPG/POPC LUV results in appearance of characteristic FRET peaks, corresponding to the contribution of the donor in the excitation spectrum of the acceptor (top) and that of the acceptor in the emission spectrum of the donor (bottom). Because the dyes attached to residues 132 of various subunits are in direct contact with each other, the formation of the trimer causes an additional FRET-independent decrease in fluorescence intensity. To account for this change, the data for the Ca^{2+}-bound form of this mutant were normalized to the quantum yield of the acceptor. The appearance of characteristic FRET peaks is reversed by removing Ca^{2+}, demonstrating the absolute reversibility of the monomer−trimer transition.

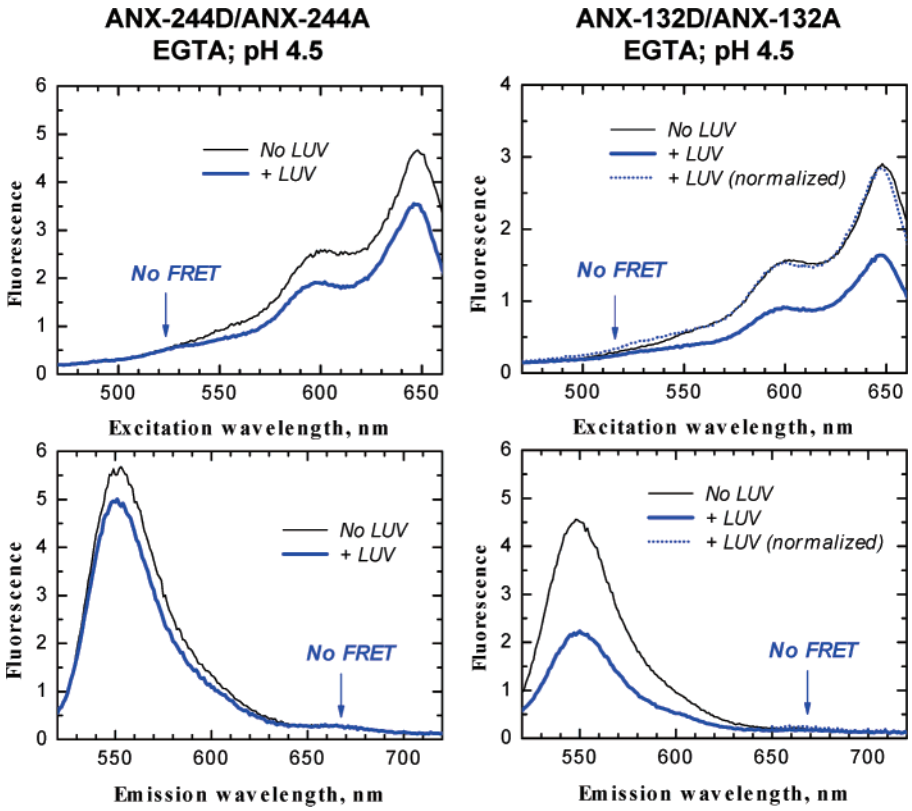

FIGURE 4: FRET experiment using the pH-inserted state of annexin to establish the aggregation state of the transmembrane form. Excitation (top panels) and emission (bottom panels) spectra are measured for a mixture of donor- and acceptor-labeled annexin mutants N244C (left panels) and K132C (right panels) in the presence and absence of POPG/POPC LUV at pH 4.5 in the absence of free Ca^{2+}. The absence of characteristic FRET peaks upon addition of POPG/POPC LUV (compare to Figure 3) indicates that a transmembrane state formed at low pH is a monomer (see the text for details).

for this quenching, the spectra were corrected for the quantum yield of the acceptor. These corrected spectra for ANX-132 (Figure 3, right panels, red dotted lines), along with uncorrected spectra for ANX-244 (Figure 3, left panels, red lines), establish important reference points for spectral changes resulting from FRET for dye-labeled ANX mutants in this well-defined model system.

Examining the Oligomeric State of Transmembrane ANX. After the spectroscopic hallmarks of FRET were established using Ca^{2+}-induced interfacial binding of ANX, the same experimental scheme was used to examine the oligomeric state of the transmembrane form (*14*, *30*) at pH 4.5 in the absence of Ca^{2+}. In the absence of membranes, the spectra of mixtures of ANX-D and ANX-A exhibited no change when the pH was reduced from 7 to 4.5, indicating that ANX remains monomeric. Addition of lipid vesicles, and resulting membrane insertion, lead to some decrease in the signal intensity (more pronounced for ANX-132, Figure 4). These changes, however, are not accompanied by a noticeable increase in the magnitude of the FRET-associated signal in the spectral regions identified by arrows (compare to Figure 3). Even after a correction for the decrease in quantum yield of the acceptor upon membrane insertion (dotted blue lines), both excitation and emission spectra show marginal additional intensity where the FRET-associated signal is expected (compare to Figure 3). A small amount of FRET could be explained by a chance colocalization of donor- and acceptor-labeled ANX in proximity with one another on the same vesicle. The behavior of another mutant, ANX-244 (Figure 4, left panels), or that of a mixed sample, with the donor and acceptor attached to different mutants (not shown), was similar: no significant FRET signal is observed. There are two general explanations for the lack of FRET. (a) The low-pH transmembrane state of ANX is a monomer. (b) The transmembrane state is an oligomer, but the labeling sites for the donor and acceptor are separated by a distance (>90 Å) far exceeding the R_0. We can discard the latter possibility, because of the relatively small size of the ANX, and because we know that the labeling sites are very close to the end of transmembrane helices making a part of a pore, and thus would have to be in proximity if the pore were comprised of an oligomer (see the Discussion).

Reversibility of Conformational and Oligomeric Changes of Membrane-Bound ANX. The first indication that insertion of ANX might be reversible was given by the mobility measurements of the EPR probe attached to the side chain of Cys144 of a single-cysteine mutant (*14*). The nature of the EPR experiment, however, did not allow a free manipulation of the sample, and the reversible insertion was shown after lipid vesicles and protein were separated by centrifugation. To observe reversible insertion of ANX under conditions where folding studies could be carried out, we have utilized the same mutant labeled with the fluorescent probe NBD, ANX-144NBD. NBD fluorescence is highly sensitive to the polarity of the probe's environment. Because residue 144 is in a solvent-exposed loop, the fluorescence of ANX-144NBD in the water-soluble form of this protein is highly quenched and has a maximum around 536 nm (curve 1 in Figure 5). When the protein assumes the transmembrane form following addition of PS/PC LUV at pH 4.5, the spectrum

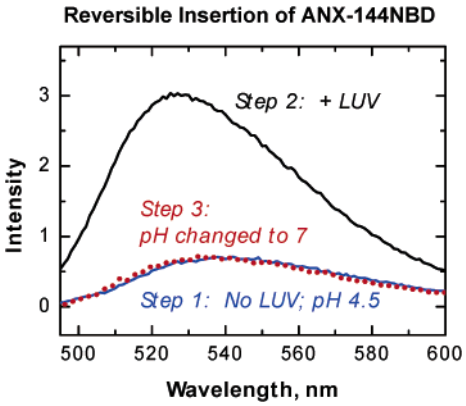

FIGURE 5: Reversibility of membrane insertion of ANX probed by fluorescence. The NBD probe was attached to a single-cysteine mutant of ANX at position 144 near the middle of a known transmembrane region. In soluble form, this site is exposed to water, resulting in low intensity (curve 1). Addition of PS/PC LUV at low pH results in deep membrane insertion of the probe, causing increased intensity and spectral shift (curve 2). Changing the pH to 7 by addition of a small amount of concentrated buffer completely reverses fluorescence changes (curve 3, corrected for dilution).

is shifted to 527 nm and the intensity is increased substantially (curve 2). Increasing the pH to 7 by addition of an aliquot of a concentrated high-pH buffer caused the protein to dissociate from the membrane, and the spectral changes are completely reversed (curve 3, dotted red line). Similar though less ideal reversibility was observed with POPG/POPC LUV (not shown).

The following experiments exploited the distinctive spectral features of the interfacial trimer and the transmembrane forms of ANX in an effort to examine the conformational reversibility of these two forms. Samples containing donor- and acceptor-labeled ANX were mixed with PS/PC LUV under conditions promoting formation of either (1) a surface trimer (pH 7, 1 mM Ca^{2+}) or (2) a transmembrane-inserted monomer (pH 4.5 in the presence of EGTA). The results were the same as those for POPC/POPG LUV shown in Figures 3 and 4: oligomerization-related FRET for the surface trimer (Figure 6, top panel, thick line) and the absence of FRET in the monomeric transmembrane form (Figure 6, bottom panel, thick line). After a prolonged incubation of 18 h, the conditions were reversed by adding appropriate amounts of acidic buffer, followed by EGTA, to the first sample, or of basic buffer followed by Ca^{2+} to the second sample (see the details in Experimental Procedures). This resulted in the corresponding loss or gain of a FRET-associated contribution of donor excitation observed below 550 nm (Figure 6, thin traces), for the first (top panel) or second sample (bottom panel), respectively. Thus, the changes in excitation spectra indicate the reversible nature of the conformational change associated with the change in oligomeric state.

DISCUSSION

The most important results of this study are (1) demonstrating that the transmembrane state of ANX at low pH is a monomer and (2) establishing the reversibility of conformational and oligomeric changes of ANX on membranes. Establishing the reversibility of a certain transition is a prerequisite for its thermodynamic characterization. Understanding the energetics of establishing a transmembrane

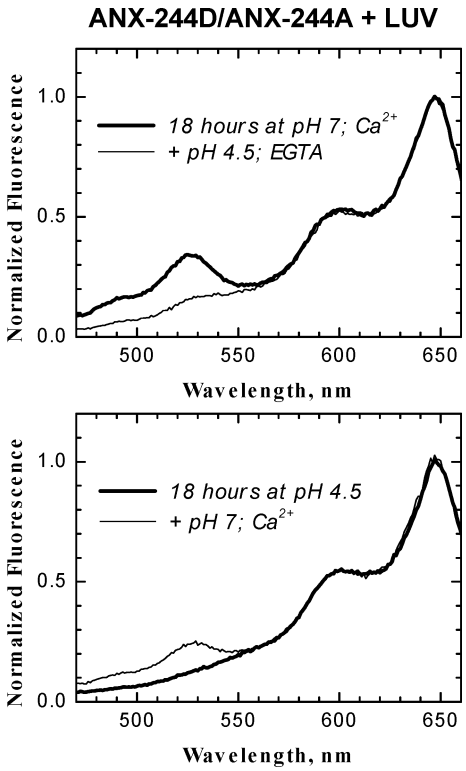

FIGURE 6: Reversibility of transitions between the Ca^{2+}-bound trimer and low-pH-inserted monomer of ANX (see Figure 1). A mixture of donor and acceptor-labeled ANX-244 was incubated in the presence of PS/PC LUV for 18 h under conditions favoring either the surface trimer (pH 7, 0.3 mM Ca^{2+}, thick line, top panel) or the transmembrane monomer (pH 4.5, EGTA, thick line, bottom panel). Then the conditions were reversed to favor another form by reducing the pH (top panel), or increasing the pH and adding Ca^{2+} (bottom panel). After 18 h, the spectra were recorded again (thin lines), revealing the reversibility of the oligomerization of ANX.

structure is an essential step in deciphering the membrane protein problem. Recently, one of us had demonstrated how thermodynamic information about membrane protein insertion and stability can be obtained using another spontaneously inserting protein, diphtheria toxin T-domain (*13*). ANX appears to be an even more suitable model for studies of membrane insertion, because, as demonstrated here (Figure 4), it is monomeric in both water-soluble and transmembrane states.

We have used FRET methodology to probe the oligomeric state of ANX. Alexa dyes, selectively attached to two single-cysteine mutants (Figure 1B), provide a number of important advantages over conventional donor−acceptor pairs. A rather high extinction coefficient and a long-wavelength position of absorbance of acceptor (Alexa-647) ensure a relatively large R_0 (~55−60 Å) even under conditions of modest spectral overlap with emission of the donor (Alexa-532). The latter, in turn, allows for a better spectral separation of donor and acceptor fluorescence. A complete lack of a direct contribution of the donor's fluorescence at 680 nm makes excitation spectra collected at this emission wavelength very sensitive to the presence of FRET. To further increase the sensitivity, we have used cross-oriented polarizers, because energy transfer causes strong depolarization of emitted light.

First, we tested our FRET approach using a well-known Ca^{2+}-induced formation of ANX trimers on membrane interfaces (*24*). As expected, addition of Ca^{2+} to a mixture

of donor- and acceptor-labeled ANX resulted in the appearance of characteristic FRET peaks in both excitation and emission spectra (Figure 3). FRET efficiency is higher for labels attached at position 132 than for those at position 244, as can be judged by the degree of the decrease in donor emission. This is roughly consistent with the proximity of the labeling sites (Figure 1B), although exact measurement of FRET efficiency is complicated by a number of factors, such as the variation in the quantum yield of dyes, complex stoichiometry, and interference from possible homotransfer of excitation energy between identical fluorophores. These factors, however, do not prevent the determination of the existence of FRET (homotransfer is actually likely to enhance the sensitivity), and thus do not affect any of the conclusions of our study. Although the design of the FRET experimental approach used herein is not optimal for quantitation of oligomerization (e.g., determination of the fraction of the oligomeric form or its stoichiometry), it is tuned to maximize sensitivity for the detection of oligomers. Because of this exquisite sensitivity, the absence of a FRET signal is a clear indicator of the lack of oligomer formation. Using this method we recently showed that annexins 1 and 2 do not form Ca^{2+}-dependent trimers on membranes (*41*).

Second, we investigated the oligomeric state of membrane-inserted ANX at low pH using the same experimental FRET protocol. There is substantial support for the transmembrane pore model shown in Figure 1, but it was not known whether all the transmembrane helices of a given pore were derived from a single annexin molecule or from an oligomer. To address this question, we placed fluorescent probes approximately five residues from the cis side of two previously identified transmembrane helices (*14*, *30*; J. M. Isas, H. T. Haigler, and R. Langen, unpublished results). The cis side locations were thought to pose a low risk of disrupting the insertion process. Furthermore, the proximity of the probes to the transmembrane helices made them ideal reporters for the formation of an oligomer consisting of transmembrane regions from different annexin molecules. We illustrate this with simple model building which considers two limiting cases of arranging a multimeric pore. The first case assumes the highest multiplicity where every helix in a pore comes from a different polypeptide chain. The distance between the centers of the tightly packed helices is equal to their diameter, which for an average transmembrane helix is ~10 Å. Even after we add an additional 10 Å to account for possible movement of labeled sites with respect to the helix center, the distance between the donor and acceptor is far shorter than R_0. The second case assumes the lowest multiplicity of the pore, which is a dimer. For an eight-helix pore, simple geometric considerations reveal that in this case the largest separation between the helices is still only ~30 Å. Even if we assume twice the separation (which is quite unlikely given the size of the protein), we still should see strong FRET, comparable to that observed for Ca^{2+}-bound ANX-244 (Figure 3), for which the distance between the donor and acceptor is ~64 Å (Figure 1). Clearly, we do not see anything like that for the transmembrane form of ANX (Figure 4).

The clear lack of FRET in our experiments unequivocally indicates that the previously characterized transmembrane pore formed by ANX is a monomer. Of course it is possible that other populations of ANX structures coexist with the structure that forms the transmembrane pore. While these putative structures theoretically could have extended conformations that permitted the formation of multimers in which FRET would not be detected, this is unlikely, because the R_0 of our two donor−acceptor pairs is greater than the diameter of a globular protein the size of ANX. In summary, our data clearly indicate that the transmembrane form of ANX with ion channel activity depicted in Figure 1 is a monomer.

For ANX to be a useful model system for studying the thermodynamics of insertion of a protein into membranes, insertion must be reversible. Two published studies showed that ANX could be inserted into phospholipid vesicles under mildly acidic conditions, extracted by increasing the pH, and then bound to vesicles in a Ca^{2+}-dependent manner at neutral pH (*14*, *29*). One method by which this process was monitored used a derivative of ANX that contained a nitroxide probe attached to residue 144. Since this residue is on an exposed loop in the aqueous form, buried in the membrane-inserted form, and at the protein−membrane interface in the Ca^{2+}-dependent form, it gave distinctive EPR signals for each of the three forms (*14*, *25*). Studies with this spin-labeled ANX were consistent with the transitions being reversible; however, the experimental procedures required that the ANX bound to vesicles be pelleted by centrifugation, extracted, and then incubated with another set of vesicles. Because of the complexity of the manipulations in these experiments, it was not possible to determine whether reversibility was complete. In this study, we have attached the polarity-sensitive fluorescent probe, NBD, to residue 144 and used this derivative to analyze reversibility. Because of the sensitivity of the fluorescence methods, the entire reversibility experiment could be performed in the same cuvette. Using this exquisitely sensitive protocol, we found that the spectra before and after insertion coincide completely (Figure 5, curves 1 and 3), thereby proving complete reversibility of transbilayer insertion of ANX as indicated by a probe that monitors the local fold. We also used a FRET assay for trimer formation to monitor the ability of inserted ANX to refold, an assay that is likely to monitor global refolding of the protein because trimer formation should require the correct conformation over extended areas of the protein. Using this assay, we showed that the transbilayer form of ANX could be extracted at neutral pH and then induced to form trimers by addition of Ca^{2+} (Figure 6).

While the exact physiological role of transmembrane insertion of ANX awaits clarification, apparently similar pH-dependent transitions play an important role in other biological processes, such as viral fusion (*39*) and action of bacterial toxins (*5*, *7*, *8*). For example, diphtheria toxin enters the cytosol after membrane insertion and translocation are triggered by endosomal acidification (*4*). This process appears to be ensured by spontaneous refolding and insertion of the translocation domain (T-domain) at low pH, and is still poorly understood on a molecular level. The insertion pathway of T-domain, however, is likely to be more complicated than that of ANX, since T-domain, unlike ANX, will bind membranes at neutral pH (*13*). Also, T-domain aggregates in solution at low pH, while ANX does not. The monomeric nature of ANX in water-soluble and transmembrane states, as well as the reversible nature of its membrane

insertion, makes it a potentially useful model system for studies of membrane protein folding and stability in general, and pH-triggered bilayer insertion in particular.

REFERENCES

1. Pfanner, N., and Truscott, K. N. (2002) Powering mitochondrial protein import, *Nat. Struct. Biol. 9*, 234−236.
2. Johnson, A. E., and van Waes, M. A. (1999) The translocon: A dynamic gateway at the ER membrane, *Annu. Rev. Cell Dev. Biol. 15*, 799−842.
3. Johnson, A. E., and Haigh, N. G. (2000) The ER translocon and retrotranslocation: Is the shift into reverse manual or automatic? *Cell 102*, 709−712.
4. Oh, K. J., Senzel, L., Collier, R. J., and Finkelstein, A. (1999) Translocation of the catalytic domain of diphtheria toxin across planar phospholipid bilayers by its own T domain, *Proc. Natl. Acad. Sci. U.S.A. 96*, 8467−8470.
5. Hoch, D. H., Romero-Mira, M., Ehrlich, B. E., Finkelstein, A., DasGupta, B. R., and Simpson, L. L. (1985) Channels formed by botulinum, tetanus, and diphtheria toxins in planar lipid bilayers: Relevance to translocation of proteins, *Proc. Natl. Acad. Sci. U.S.A. 82*, 1692−1696.
6. Arnon, S. S., Schechter, R., Inglesby, T. V., Henderson, D. A., Bartlett, J. G., Ascher, M. S., Eitzen, E., Fine, A. D., Hauer, J., Layton, M., Lillibridge, S., Osterholm, M. T., O'Toole, T., Parker, G., Perl, T. M., Russell, P. K., Swerdlow, D. L., and Tonat, K. (2001) Botulinum toxin as a biological weapon: Medical and public health management, *JAMA, J. Am. Med. Assoc. 285*, 1059−1070.
7. Neale, E. A. (2003) Moving across membranes, *Nat. Struct. Biol. 10*, 2−3.
8. Koriazova, L. K., and Montal, M. (2003) Translocation of botulinum neurotoxin light chain protease through the heavy chain channel, *Nat. Struct. Biol. 10*, 13−18.
9. Matouschek, A., Kellis, J. T., Serrano, L., and Fersht, A. R. (1989) Mapping the transition state and pathway of protein folding by protein engineering, *Nature 340*, 122−126.
10. Gilmanshin, R., Williams, S., Callender, R. H., Woodruff, W. H., and Dyer, R. B. (1997) Fast events in protein folding: Relaxation dynamics of secondary and tertiary structure in native apomyoglobin, *Proc. Natl. Acad. Sci. U.S.A. 94*, 3709−3713.
11. Shortle, D., Stites, W. E., and Meeker, A. K. (1990) Contributions of the large hydrophobic amino acids to the stability of staphylococcal nuclease, *Biochemistry 29*, 8033−8041.
12. Shortle, D. (1995) Staphylococcal nuclease: A showcase of m-value effects, *Adv. Protein Chem. 46*, 217−248.
13. Ladokhin, A. S., Legmann, R., Collier, R. J., and White, S. H. (2004) Reversible refolding of the diphtheria toxin T-domain on lipid membranes, *Biochemistry 43*, 7451−7458.
14. Langen, R., Isas, J. M., Hubbell, W. L., and Haigler, H. T. (1998) A transmembrane form of annexin XII detected by site-directed spin labeling, *Proc. Natl. Acad. Sci. U.S.A. 95*, 14060−14065.
15. Moss, S. E., and Morgan, R. O. (2004) The annexins, *Genome Biol. 5*, 219−219.8.
16. Rescher, U., and Gerke, V. (2004) Annexins: Unique membrane binding proteins with diverse functions, *J. Cell Sci. 117*, 2631−2639.
17. Rand, J. H. (1999) "Annexinopathies": A new class of diseases, *N. Engl. J. Med. 340*, 1035−1036.
18. Oh, P., Li, Y., Yu, J. Y., Durr, E., Krasinska, K. M., Carver, L. A., Testa, J. E., and Schnitzer, J. E. (2004) Subtractive proteomic mapping of the endothelial surface in lung and solid tumours for tissue-specific therapy, *Nature 429*, 629−635.
19. Seaton, B. A. (1996) *Annexins: Molecular Structure to Cellular Function*, R. G. Landes, Austin, TX.
20. Swairjo, M. A., Concha, N. O., Kaetzel, M. A., Dedman, J. R., and Seaton, B. A. (1995) Ca^{2+}-bridging mechanism and phospholipid head group recognition in the membrane-binding protein annexin V, *Nat. Struct. Biol. 2*, 968−974.
21. Kaetzel, M. A., Mo, Y. D., Mealy, T. R., Campos, B., Bergsma-Schutter, W., Brisson, A., Dedman, J. R., and Seaton, B. A. (2001) Phosphorylation mutants elucidate the mechanism of annexin IV-mediated membrane aggregation, *Biochemistry 40*, 4192−4199.
22. Oling, F., Sopkova-de Oliveira Santos, J., Govorukhina, N., Mazères-Dubut, C., Bergsma-Schutter, W., Oostergetel, G., Keegstra, W., Lambert, O., Lewit-Bentley, A., and Brisson, A. (2000) Structure of membrane-bound annexin A5 trimers: A hybrid cryo-EM-X-ray crystallography study, *J. Mol. Biol. 304*, 561−573.
23. Reviakine, I., Bergsma-Schutter, W., Mazères-Dubut, C., Govorukhina, N., and Brisson, A. (2000) Surface topography of the p3 and p6 annexin V crystal forms determined by atomic force microscopy, *J. Struct. Biol. 131*, 234−239.
24. Langen, R., Isas, J. M., Luecke, H., Haigler, H. T., and Hubbell, W. L. (1998) Membrane-mediated assembly of annexins studied by site-directed spin labeling, *J. Biol. Chem. 273*, 22453−22457.
25. Isas, J. M., Langen, R., Hubbell, W. L., and Haigler, H. T. (2004) Structure and dynamics of a helical hairpin that mediates calcium-dependent membrane binding of annexin B12, *J. Biol. Chem. 279*, 32492−32498.
26. Isas, J. M., Patel, D. R., Jao, C., Jayasinghe, S., Cartailler, J.-P., Haigler, H. T., and Langen, R. (2003) Global structural changes in annexin 12: The roles of phospholipid, Ca^{2+}, and pH, *J. Biol. Chem. 278*, 30227−30234.
27. Gerke, V., and Moss, S. E. (2002) Annexins: From structure to function, *Physiol. Rev. 82*, 331−371.
28. Isas, J. M., Langen, R., Haigler, H. T., and Hubbell, W. L. (2002) Structure and dynamics of a helical hairpin and loop region in annexin 12: A site-directed spin labeling study, *Biochemistry 41*, 1464−1473.
29. Isas, J. M., Cartailler, J.-P., Sokolov, Y., Patel, D. R., Langen, R., Luecke, H., Hall, J. E., and Haigler, H. T. (2000) Annexins V and XII insert into bilayers at mildly acidic pH and form ion channels, *Biochemistry 39*, 3015−3022.
30. Ladokhin, A. S., Isas, J. M., Haigler, H. T., and White, S. H. (2002) Determining the membrane topology of proteins: Insertion pathway of a transmembrane helix of annexin 12, *Biochemistry 41*, 13617−13626.
31. Haugland, R. P. (1996) *Handbook of Fluorescent Probes and Research Chemicals*, Molecular Probes, Eugene, OR.
32. Mayer, L. D., Hope, M. J., and Cullis, P. R. (1986) Vesicles of variable sizes produced by a rapid extrusion procedure, *Biochim. Biophys. Acta 858*, 161−168.
33. Hope, M. J., Bally, M. B., Mayer, L. D., Janoff, A. S., and Cullis, P. R. (1986) Generation of multilamellar and unilamellar phospholipid vesicles, *Chem. Phys. Lipids 40*, 89−107.
34. Lakowicz, J. R. (1983) *Principles of Fluorescence Spectroscopy*, Plenum Press, New York.
35. Wolber, P. K., and Hudson, B. S. (1979) An analytic solution to the Förster energy transfer problem in two dimensions, *Biophys. J. 28*, 197−210.
36. Davenport, L., Dale, R. E., Bisby, R. H., and Cundall, R. B. (1985) Transverse location of the fluorescent probe 1,6-diphenyl-1,3,5-hexatriene in model lipid bilayer membrane systems by resonance excitation energy transfer, *Biochemistry 24*, 4097−4108.
37. Ladokhin, A. S., Malak, H., Johnson, M. L., Lakowicz, J. R., Wang, L., Steggles, A. W., and Holloway, P. W. (1992) Frequency-domain fluorescence of mutant cytochrome b_5, in *Time-Resolved Laser Spectroscopy in Biochemistry* (Lakowicz, J. R., Ed.) Vol. III, pp 562−569, SPIE, Bellingham, WA.
38. Wimley, W. C., and White, S. H. (2000) Determining the membrane topology of peptides by fluorescence quenching, *Biochemistry 39*, 161−170.
39. Tamm, L. K., Han, X., Li, Y., and Lai, A. L. (2002) Structure and function of membrane fusion peptides, *Biopolymers 66*, 249−260.
40. Luecke, H., Chang, B. T., Mailliard, W. S., Schlaepfer, D. D., and Haigler, H. T. (1995) Crystal structure of the annexin XII hexamer and implications for bilayer insertion, *Nature 378*, 512−515.
41. Patel, D. R., Isas, J. M., Ladokhin, A. S., Jao, C. C., Kim, Y. E., Kirsch, T., Langen, R., and Haigler, H. T. (2005) The conserved core domains of annexins A1, A2, A5, and B12 can be divided into two groups with different Ca^{2+}-dependent membrane-binding properties, *Biochemistry 44*, in press.

BI047805U